Influence of ions on two-dimensional and three-dimensional atomic force microscopy at fluorite-water interfaces

doi: 10.1088/1361-6528/aa7188

Influence of ions on two-dimensional and three-dimensional atomic force microscopy at fluorite-water interfaces

K. Miyazawa[1], M. Watkins[2], A. L. Shluger[3] and T. Fukuma[1,4]

[1] Division of Electrical Engineering and Computer Science, Kanazawa University, Kakuma-machi, Kanazawa 920-1192, Japan

[2] School of Mathematics and Physics, University of Lincoln, Brayford Pool, Lincoln LN6 7TS, United Kingdom

[3] Department of Physics and Astronomy and London Centre for Nanotechnology, University College London, Gower Street, London, WC1E 6BT, United Kingdom

[4] ACT-C, Japan Science and Technology Agency, Honcho 4-1-9, Kawaguchi 332-0012, Japan

E-mail: fukuma@staff.kanazawa-u.ac.jp

Abstract. Recent advancement in liquid-environment atomic force microscopy (AFM) has enabled us to visualize three-dimensional (3D) hydration structures as well as two-dimensional (2D) surface structures with subnanometer-scale resolution at solid-water interfaces. However, the influence of ions present in solution on the 2D- and 3D-AFM measurements has not been well understood. In this study, we perform atomic-scale 2D- and 3D-AFM measurements at fluorite-water interfaces in pure water and supersaturated solution of fluorite. The images obtained in these two environments are compared to understand the influence of the ions in solution on these measurements. In the 2D images, we found clear difference in the nanoscale structures but no significant difference in the atomic-scale contrasts. However, the 3D force images show clear difference in the subnanometer-scale contrasts. The force contrasts measured in pure water largely agree with those expected from the molecular dynamics simulation and the solvent tip approximation model. In the supersaturated solution, an additional force peak is observed over the negatively charged fluorine ion site. This location suggests that the observed force peak may originate from cations adsorbed on the fluorite surface. These results demonstrate that the ions can significantly alter the subnanometer-scale force contrasts in the 3D-AFM images.

1. Introduction

Water and ions play important roles in many of the solid-liquid interfacial phenomena, including crystal growth [1], biomolecular interactions [2–4], and electrochemical reactions [5]. Thus, methods to measure their atomic- or molecular-scale behavior are required in a wide range of research fields. To date, spectroscopic methods such as X-ray [6], neutron [7] and optical beam [8] technologies have been widely used for

investigating distributions of water and ions at solid-liquid interfaces. While these methods have a subnanometer-scale vertical resolution, their lateral resolution is a few orders of magnitude larger than the atomic scale. This drawback often hinders an atomistic understanding of interface structures and processes and direct comparison of the results obtained by experiments and atomistic simulations.

Atomic force microscopy (AFM) [9] is one of the most promising candidates to overcome this limitation as it has a subnanometer-scale resolution both in the vertical and lateral directions. Owing to the recent advancements in the AFM instrumentation, such an atomic-scale measurement is possible even in liquid [10, 11] as well as in vacuum [12, 13]. Moreover, several research groups developed three-dimensional (3D) force measurement techniques [14, 15], where the tip is scanned both in the vertical and lateral directions and the force applied to the tip during the scan is recorded to produce a 3D force image. Previous studies revealed significant similarities between the experimentally measured 3D force images and the theoretically simulated hydration structures at some of the model solid-liquid interfaces [14–17]. This agreement has stimulated further studies on direct 3D measurements of hydration structures by AFM.

Till date, majority of the atomic-scale measurements in liquid by dynamic-mode AFM have been performed in an electrolytic solution because an atomic-scale AFM measurement in pure water is typically much more difficult than that in an electrolytic solution [18–20]. Nevertheless, the obtained results are often compared with a theoretically simulated water density or force images without taking into account the influence of ions present in the electrolyte. Recently, one solution for this problem was reported, where a small cantilever with a resonance frequency (f_0) of ∼3.5 MHz in liquid [21] was used for obtaining a subnanometer-scale 3D force image even in pure water. The force image measured on a calcite ($CaCO_3$) ($10\bar{1}4$) surface in pure water was compared with the one obtained by an atomistic MD simulation [22], which clarified the central issues underpinning the mechanism of 3D hydration structure measurements [19]. The small cantilever was also used for imaging the 3D force distribution on a fluorite (CaF_2) (111) surface in pure water [23]. The obtained image was compared with the force image calculated by the solvation tip approximation (STA) model [24, 25], where a tip is approximated by a single water molecule. This comparison showed that a force and a water density distribution can be significantly different and hence conversion from the water density to the force by the STA model is recommended as the current best practice for their comparison.

As discussed above, the experimental techniques and the theoretical basis for the hydration structure measurements in pure water are making steady progress towards their establishment. In the meanwhile, many of the interesting interfacial phenomena take place in an electrolytic solution. Hence, it is necessary to understand the influence of ions on the measurements of hydration structures. So far, several research groups compared atomic-scale contrasts of the two-dimensional (2D) AFM images obtained in pure water and an electrolytic solution [26–29]. They suggested the formation of stable adsorption structures of cations on a mica or a calcite surface. As for the influence

of ions on a 3D force image, there is only one experimental study [30], where the 3D force images of a mica-water interface obtained in 0.2 M was compared with that in 4 M KCl solution, which is close to the saturated concentration. These results suggested that the ions form a 3D adsorption structure with a surprisingly high thickness (> 3 nm) under such an extremely high ionic concentration. Although these previous studies suggest the significant influence of ions on the measurements of hydration structures, the number of such studies are still limited. In particular, detailed comparison between 3D force images obtained in pure water and in a moderate electrolytic solution (< 1 M) has not been reported. Since most of the important interfacial phenomena studied in biology or electrochemistry take place in a moderate electrolytic solution, such studies are of particular importance.

Fluorite (111) surface was widely used as a model system for investigating the imaging mechanism of atomic-resolution AFM in ultra-high vacuum (UHV) from experimental and theoretical aspects [31–34]. In addition, the growth mechanism of a fluorite crystal in aqueous solution was extensively studied in relation to the fabrication of optical components [35–38], formation of tooth enamel [39, 40] and biomineralization [41–46]. Thus, the theoretical basis for atomistic molecular dynamics (MD) simulation of the fluorite-water interface was relatively well-established. Therefore, some of the early simulation studies on the imaging mechanism of atomic-resolution liquid-environment AFM were performed with a model of this interface [22, 47, 48]. To compare the results obtained by simulation and experiments, we previously performed systematic AFM experiments at this interface with different CaF_2 concentration and pH [49]. Among the many conditions tested, we found only two conditions that allow us to perform atomic-scale measurements at this interface: in pure water but within 20 min after the immersion or in a supersaturated solution of CaF_2 ($\sigma = 100$). σ denotes the degree of supersaturation and defined by $\sigma = (c - c_{\mathrm{eq}})/c_{\mathrm{eq}}$, where c and c_{eq} are the concentrations of the solution used for the experiment and saturated solution, respectively. For the 3D force images obtained in pure water, we previously reported detailed comparison with the simulated 3D images [23]. In contrast, 3D force images obtained in a supersaturated solution have not been reported. Furthermore, detailed comparison between the measurements in water and a supersaturated solution have not been reported even for the 2D imaging.

In this study, we perform 2D and 3D AFM measurements at fluorite-water interfaces in pure water and supersaturated solution ($\sigma = 100$). We compare the obtained images with the theoretically simulated water density and force images and clarify their differences. We discuss possible origins of the differences in relation to the influence of the ions. Through these discussions, we also demonstrate the importance of the 3D analysis for investigating the influence of ions on the hydration structure measurements by AFM.

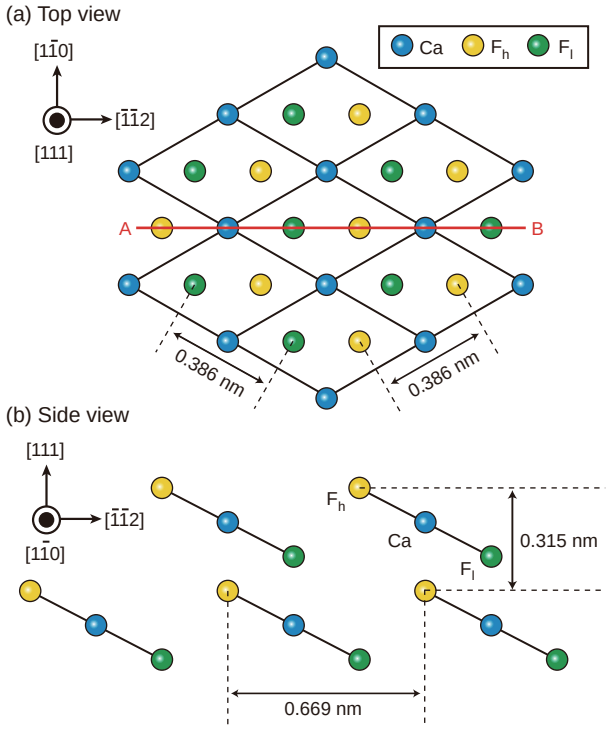

Figure 1. Atomistic model of the fluorite (111) surface. (a) Top view. (b) Side view.

2. Methods

2.1. Sample preparation

The fluorite (111) surface consists of hexagonally arranged Ca^{2+} and F^- ions as shown in Fig. 1a. Figure 1b shows the cross sectional model of the fluorite crystal taken along line AB shown in Fig. 1a. This figure shows that the fluorite crystal consists of F^-–Ca^{2+}– F^- layers stacked in the [111] direction with a spacing of 0.315 nm. Here, we refer to F^- ions higher and lower than the Ca^{2+} ions as F_h and F_l ions, respectively. All of the three ions (Ca, F_h and F_l) are located along the line AB in Fig. 1a. Thus, we mainly analyzed the cross sections of the 3D force and water density images obtained along the line AB for understanding the local distribution over these different ions.

We used a commercially available fluorite (111) substrate with the size of 10 × 10 × 2 mm^3 (Crystal Base). We fixed the fluorite substrate to a sample holder by glue. We cleaved the fluorite (111) substrate with a razor blade just before an AFM experiment, and quickly dropped an imaging solution (50 μL) onto the substrate with its surface in the upright direction. As the imaging solution, we used either milli-Q water or a supersaturated CaF_2 solution ($\sigma = 100$). Although Milli-Q water is not pure water in a strict sense, here we refer to it as pure water to discriminate it from an electrolytic solution which contains substantial amount of ions.

The supersaturated solution ($\sigma = 100$) was prepared by mixing the same amounts of 38 mM $CaCl_2$ and 76 mM KF solutions. The solution prepared in this way appears

to be transparent and does not form any visible precipitates in spite of the large degree of the supersaturation. Although we do not know the exact mechanism of preventing the precipitation, we speculate that the other ions such as K^+ and Cl^- may suppress the nucleation of a CaF_2 crystal. Note that we have strong evidence to show that the prepared solution is not a KCl solution but a supersaturated solution although it looks transparent. First, the fluorite crystal in this solution shows a rapid growth as shown later in Figure 2b. Secondly, the fluorite crystal in 100 mM KCl solution (Figure S1 in Supplementary Data) shows morphological changes similar to those in pure water (Figure 2a) but significantly different from those in the supersaturated solution (Figure 2b). Thus, we are confident that the prepared solution is not a KCl solution but a supersaturated solution of CaF_2.

2.2. AFM measurements

We used a home-built frequency modulation AFM (FM-AFM) with an ultra-low noise cantilever deflection sensor [50, 51] and a high stability photothermal excitation system [21, 52]. A commercially available phase-locked loop (PLL) circuit (OC4, SPECS) was used for oscillating a cantilever at its resonance frequency with a constant amplitude (A) and for detecting Δf induced by the force variation. The AFM head was controlled with a commercially available AFM controller (ARC2, Asylum Research). We modified the control software to perform 3D force measurements. The obtained 3D Δf images were converted to 3D force ($F_{\rm exp}$) images using the Sader's equation [53].

Among the several methods proposed for the 3D force measurements, we used 3D scanning force microscopy (3D-SFM) [14]. In this method, the tip is vertically scanned with a fast sinusoidal wave while the tip is slowly scanned in the lateral direction. During the tip scan, frequency shift (Δf) induced by the force applied to the tip is recorded to produce a 3D Δf image. The physical and pixel sizes of the original 3D Δf images were $3 \times 3 \times 1.5$ nm^3 and $64 \times 64 \times 256$ pixels, respectively. The frequency and amplitude of the z modulation and the lateral scan speed during the 3D-SFM imaging were 195.3 Hz, 1.5 nm and 9.16 nm/s, respectively. The individual 3D Δf images were obtained in 53 sec.

As discussed above, 3D force measurements in pure water are generally more difficult than those in an electrolytic solution. Thus, we used special experimental procedures and the data processing methods previously reported in detail in Ref. [23]. Here, we only describe them in short. We used an ultra-short cantilever (USC-F5-k30, Nanoworld) with f_0, quality factor (Q) and the spring constant (k) of 3.91 MHz, 9.6 and 106.0 N/m, respectively. We applied drift corrections and correlation averaging filter to the measured 3D Δf image and then converted it to the 3D $F_{\rm exp}$ image. We subtracted the long-range (LR) repulsive force component from the 3D $F_{\rm exp}$ image to obtain a 3D short-range $F_{\rm exp}$ image. Basically, these processes do not change the main contrast features in the raw data but improve their clarity.

For the other AFM experiments, we used another type of small cantilevers (AC55,

Olympus). The f_0, Q and k of the AC55 cantilever used for the 2D and 3D AFM experiments in the supersaturated solution were 1.53 MHz, 11.1 and 142.5 N/m, respectively while those for the 2D FM-AFM experiments in pure water were 1.11 MHz, 10.2 and 83.0 N/m, respectively. The F_{exp} image obtained in supersaturated solution did not show significant influence of the LR repulsive force owing to the short Debye length. Thus, we did not subtract the LR component from it. For all the measurements, the tip side of the cantilevers was coated with a 30 nm Si thin film using a dc sputter coater (K575XD, Emitech) to remove contaminants on the tip surface [18].

2.3. Simulations

The water density (ρ) distribution at a fluorite-water interface was calculated by classical MD simulation as implemented in the version 4 series of the GROMACS code [48]. To describe water, the TIP4P/2005 model was used. We applied a 0.9 nm cut-off to treat non-bonded interactions and a smooth particle mesh Ewald method to treat electrostatics. The equations of motion were integrated using a 2 fsec time step, and the LINCS algorithm was used to enforce rigid water geometries. An NPT ensemble (300 K, 1 atm) was generated using Berendsen thermostats and barostats, with the time constants of 1.0 and 10.0 psec for temperature and pressure, respectively. The first 0.5 nsec of the 4 nsec simulations were discarded as the equilibration period.

We applied a correlation averaging filter to the ρ image. We converted the filtered ρ image into the force image (F_{STA}) using the STA model [23–25]. In this model, the relationship between F_{STA} and ρ is described by

$$F_{\mathrm{STA}} = \frac{k_B T}{\rho}\frac{\partial \rho}{\partial z}, \tag{1}$$

where, k_B, T and z denote Boltzmann's constant, temperature and the vertical tip position with respect to the sample surface, respectively.

3. Results and Discussion

3.1. Comparison of 2D FM-AFM images

Figure 2 shows FM-AFM images of the fluorite (111) surface obtained in pure water and the supersaturated solution ($\sigma = 100$). The large-scale images (Figures 2(i) and 2(iii)) were taken at the same position so that they show the time-dependent changes in the surface morphology. During the imaging, we occasionally increased the magnification to see atomic-scale structures at the center of the large-scale images. Although these atomic-scale images were obtained at similar surface positions, these positions are not exactly the same due to the drift of the tip position. Thus, the obtained atomic-scale images do not show the time-dependent changes of the same surface area but are examples of many images taken with a similar condition. As mentioned above, we often changed the magnification during the imaging. Even when we changed the scan size from a small one to a large one, we did not see any trace of the previous tip scan. This

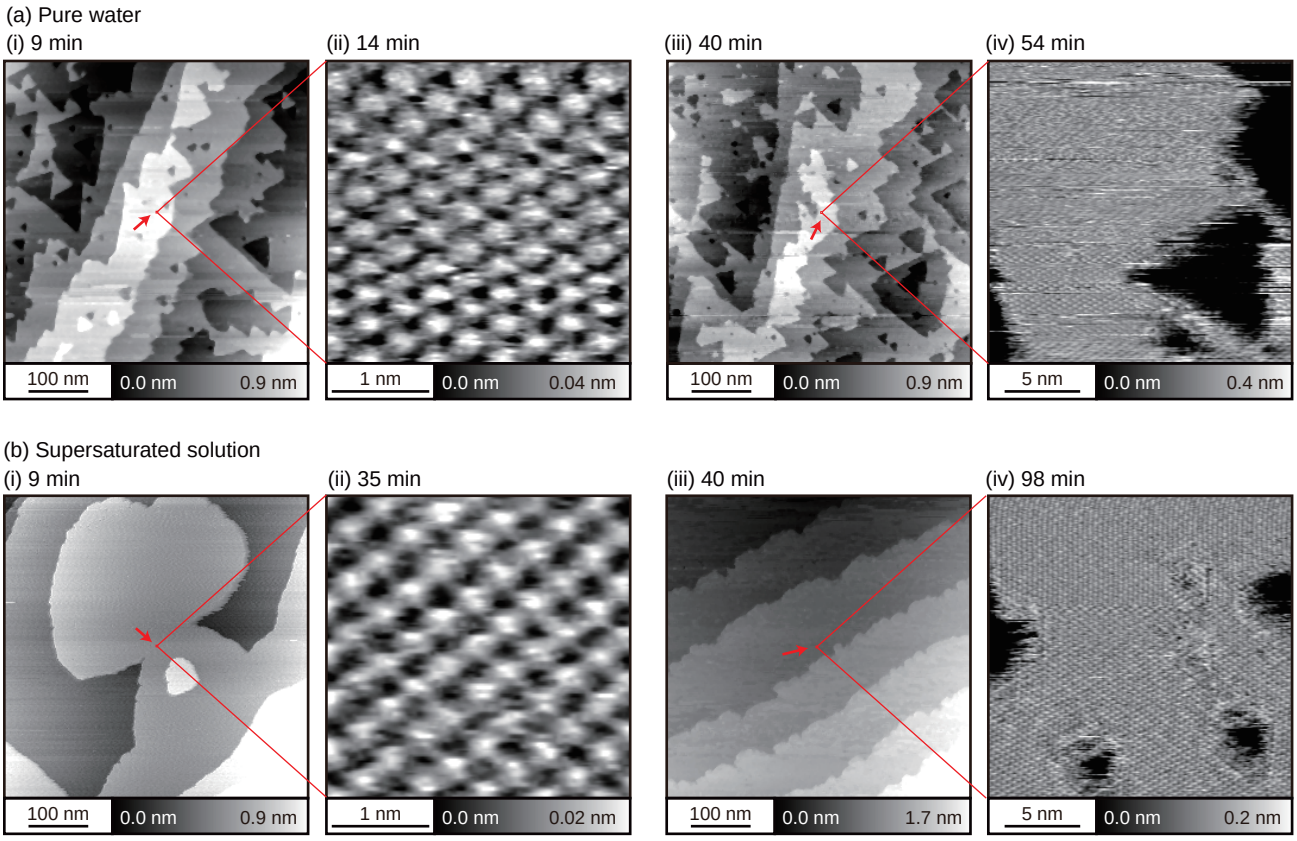

Figure 2. FM-AFM images of the fluorite (111) surface obtained in pure water and supersaturated solution ($\sigma = 100$). The time lapse since the immersion of the sample into the liquid is described in the individual figure labels. (a) In pure water. (i) $\Delta f = +3.91$ kHz. $A = 180$ pm. (ii) $\Delta f = +3.91$ kHz. $A = 217$ pm. (iii) $\Delta f = +3.91$ kHz. $A = 151$ pm. (iv) $\Delta f = +7.85$ kHz. $A = 174$ pm. (b) In the supersaturated solution ($\sigma = 100$). (i) $\Delta f = +3.91$ kHz. $A = 123$ pm. (ii) $\Delta f = +3.91$ kHz. $A = 150$ pm. (iii) $\Delta f = +3.91$ kHz. $A = 123$ pm. (iv) $\Delta f = +3.91$ kHz. $A = 120$ pm.

result suggests that the tip scan did not cause any irreversible changes in the surface morphology.

Figure 2a shows FM-AFM images of the fluorite (111) surface obtained in pure water. Within ∼20 min after the immersion of the substrate into water, the surface shows atomically flat terraces with some atomistic steps and triangular pits (Fig. 2a(i)). On the flat terraces, FM-AFM images show a hexagonally arranged atomic-scale contrast (Fig. 2a(ii)). Due to the dissolution of the surface, the step retreats at ∼4.3 nm/min on average and the densities of the steps and pits increase with time (Fig. 2a(iii)). After ∼20 min, it gradually becomes difficult to find an atomically flat area. In addition, even on such a flat area, the obtained atomic-scale images were often distorted due to the instabilities in the tip-sample distance regulation (Fig. 2a(iv)).

Previous AFM studies reported that the Ca^{2+} ions dissolved from the surface react with the OH^- ions in the solution to form calcium hydroxyl complexes [54, 55] and that such complexes often grow from the surface defects to form nanoscale islands with a

constant height (∼2.8 nm) [49,55]. In this study, we empirically found that the density of such islands strongly depends on the cleavage conditions. When the substrate is cleaved by giving an impulsive force with a razor blade in the $[1\bar{1}0]$ direction, the cleaved surface presents a relatively large area of atomically flat terraces with small number of defects and the formation of the islands is greatly suppressed. These results are consistent with the previously reported idea that the islands are grown from the surface defects.

Although the nanoscale islands were not formed on the surface, the observed instabilities of the tip-sample distance regulation suggest the existence of adsorbates that are weakly bound to the surface. Owing to the dissolved CO_2, there may be carbonate ions near the interface. Thus, these adsorbates may be either calcium hydroxides or calcium carbonates. Future experiments with a controlled environment (e.g. in N_2 or Ar gas) may help us to identify the chemical species of these adsorbates.

Figure 2b shows FM-AFM images of the fluorite (111) surface obtained in the supersaturated solution ($\sigma = 100$). At the beginning of the experiment, the surface shows a relatively large area of the atomically flat terraces and the step edges present non-uniform orientations and hence a round shape (Fig. 2b(i)). On the flat terraces, we were able to obtain FM-AFM images showing hexagonally arranged atomic-scale protrusions (Fig. 2b(ii)). Owing to the high degree of supersaturation, the steps grow rapidly but the growth rate was initially non-uniform. After several tens of minutes, the step growth rates reached a constant value (∼25.0 nm/min on average) and the step directions and the inter-step distances became almost uniform (Fig. 2b(iii)). Although the density of the surface defects increased with time, we were able to perform stable atomic-resolution imaging throughout the experiment for a few hours (Fig. 2b(iv)). This result suggests that the increase of the concentration of F^- ions hinders the formation of the calcium compounds such as $Ca(OH)_x$ or $CaCO_3$ near the surface as reported previously [49].

The large-scale FM-AFM images obtained in the two different environments clearly show the differences in the surface structures and their time-dependent changes. However, the atomic-scale FM-AFM images show similar contrasts (Figs. 2a(ii) and 2b(ii)) and do not present any significant differences. These results show that atomic-scale 2D AFM imaging does not necessarily allow us to investigate the influence of ions on the hydration structures at a solid-liquid interface.

3.2. Comparison of 3D-SFM images

Figure 3 shows the 3D images of ρ, F_{STA} and F_{exp} obtained in pure water and the supersaturated solution. For comparision between their subnanometer-scale contrasts, we extracted z cross sections from each 3D image along the line AB in Fig. 1a as shown in Fig. 4(i). The major contrast features observed in these images are schematically shown in Fig. 4(ii). Figure 4(iii) shows the z profiles measured on the Ca, F_h and F_l sites.

Before we start comparing these images, here we discuss the possible influence of

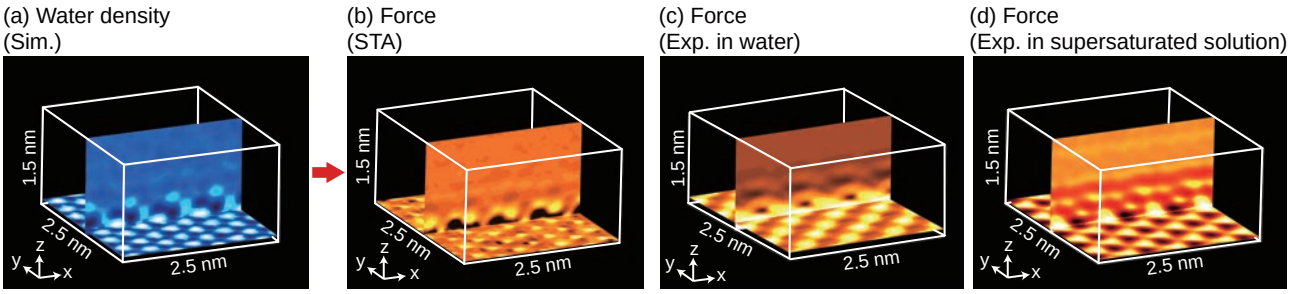

Figure 3. 3D images obtained by experiments and simulations. (a) ρ image calculated by MD simulation. (b) F_{STA} image calculated by the STA model. (c) F_{exp} image measured in pure water. (d) F_{exp} image measured in supersaturated solution. The crystallographic directions corresponding to the x, y and z axes are $[\bar{1}\bar{1}2]$, $[1\bar{1}0]$ and $[111]$, respectively.

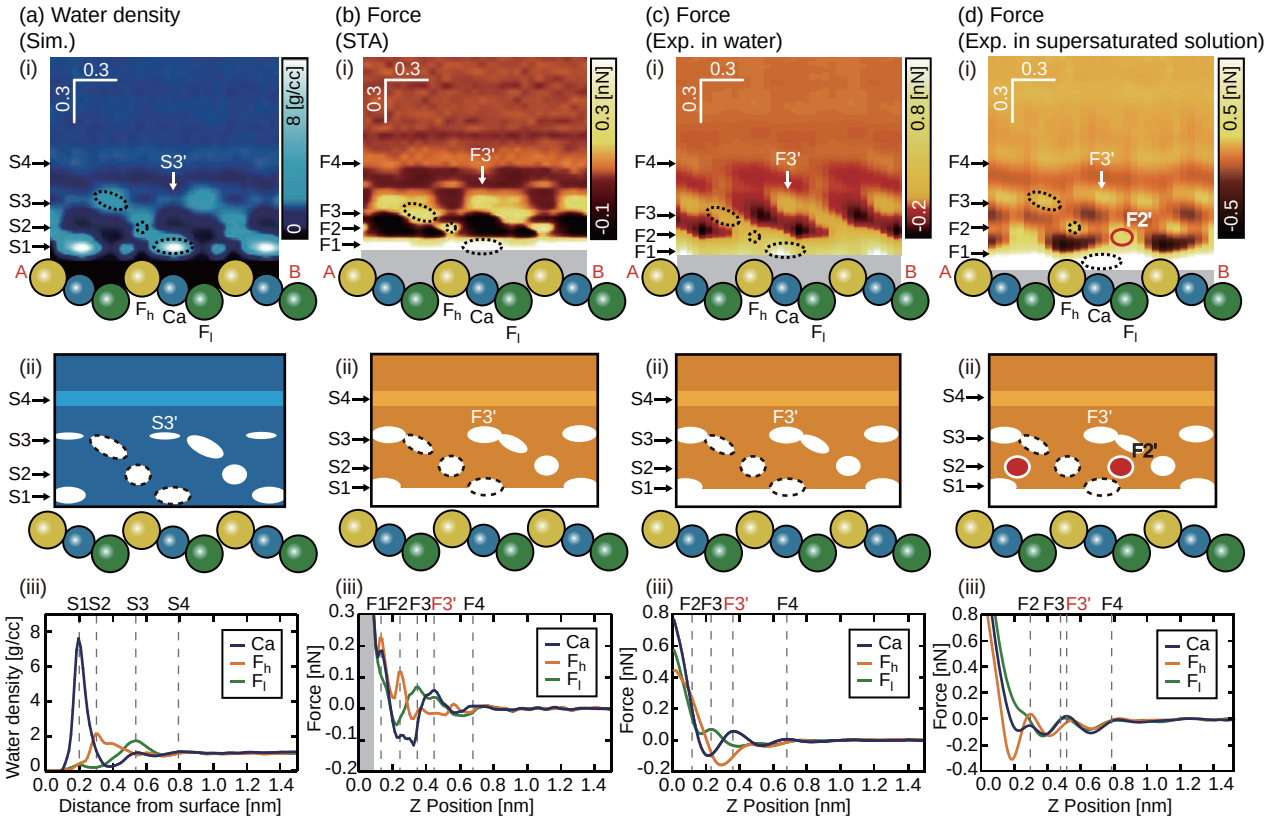

Figure 4. The results of the (a) ρ image in water calculated by MD simulation, (b) F_{STA} image calculated by STA, (c) F_{exp} image obtained by experiment in water and (d) the F_{exp} image obtained by experiment in supersaturated solution. We show (i) the z cross sections obtained from each 3D images with (ii) their schematic models of z cross sections, and (iii) z profiles obtained from each z cross sections over the surface Ca, $\mathrm{F_h}$ and $\mathrm{F_l}$ sites.

the tip on the intrinsic hydration structures. During the imaging, the tip is oscillated at 3.9 MHz for an ultra-small cantilever (USC, Nanoworld) and 1.5 MHz for a small cantilever (AC55, Olympus). In either case, the time scale of the tip movement is on the order of hundreds of nanoseconds, which is much longer than the relaxation time of water at the interface (< 1 ns). Thus, we can consider that the tip movement is quasi-static. In the meanwhile, the tip and its hydration shells affect the time-averaged density distribution of water. We previously investigated this influence by detailed comparison between the experiments and atomistic MD simulation [19] and explained why we can visualize the intrinsic 3D hydration structures even with a nanoscale tip. In addition, we also previously reported the detailed comparison between the force images obtained by the STA model and experiment [23], discussed the role of the tip hydration shell and explained that it rather helps us to probe the true hydration structure of the sample. Therefore, here we assume that the measured force distributions largely represent the true interfacial structures.

As we previously reported the detailed comparison between the first three images [23], here we only briefly summarize it as follows. The ρ image shows local hydration peaks S1–S3 over the Ca, F_h and F_l sites as indicated by the dotted lines in Fig. 4a(i). In addition, a layer-like distribution S4 is observed above these hydration peaks. These peaks are also confirmed in the z profiles of ρ. In the F_{STA} image, we can also find enhanced force contrasts (F1–F4) corresponding to S1–S4. However, the F_{STA} image shows an additional force peak F3′ next to F3. In contrast, the ρ image shows only a weak hydration peak S3′ at the corresponding position. This enhancement of the force contrast comes from the steep gradient of ρ in the z range of 0.4–0.5 nm as shown in Fig. 4a(iii). The F_{exp} image obtained in pure water shows similar contrast features to those in the F_{STA} image, where we can confirm not only F1–F4 but also F3′. This excellent agreement demonstrates the effectiveness of the STA model and the reliability of the experimental data.

To compare the F_{exp} image obtained in the supersaturated solution with the other three images, we adjusted the vertical and lateral positions of its z cross section as follows. The vertical position is adjusted so that the height of F4 is aligned to that in the other images. Just below F4, we found pairs of the local force peaks, which we assumed to be F3 and F3′. This allowed us to identify the positions of the force peaks F1–F3 as indicated by the dotted lines in Fig. 4d(i). However, the image shows another force peak F2′ as indicated by the solid circle. This difference is also confirmed in the z profiles measured over the F_l site. The force peak at F2 position appears only in the curve obtained in the supersaturated solution. Probably due to the existence of the F2′ peak, F1–F3 appear to be slightly displaced to keep sufficient distance from F2′. While the other minor differences in the image contrasts are not necessarily reproducible, the F2′ peak was reproducibly imaged even with a different tip and a sample in the supersaturated solution.

In the ρ image, there is a relatively large cavity at the position corresponding to F2′. Thus, we speculate that this spot may serve as an ideal adsorption site for an

ion. The supersaturated solution used in this experiment was prepared by dissolving $CaCl_2$ and KF in water. Hence, the solution contains Ca^{2+}, K^+, Cl^- and F^-. Due to the negative charge of the F_1 ions just under F2′, the adsorbed ions are most likely to be Ca^{2+} or K^+. Although further understanding will require a help of MD simulation with a model containing ions, our experimental result demonstrates that the ions can significantly alter subnanometer-scale contrasts in the 3D force image.

4. Conclusion

In this study, we performed subnanometer-scale 2D and 3D AFM measurements at fluorite-water interfaces in pure water and the supersaturated solution ($\sigma = 100$). In the 2D images, we found clear differences in the nanoscale structures but no significant difference in the atomic-scale contrasts. In the 3D images, a clear difference in the subnanometer-scale contrast was observed. In pure water, the force contrasts were similar to those obtained by the MD simulation and the STA model. However, the contrasts obtained in the supersaturated solution show an additional force peak over the negatively charged F_1 site. This location suggests that the observed force peak may originate from cations adsorbed on the fluorite surface.

The ultimate goal of this study is to establish an AFM method for the measurements of 3D distribution of water and ions at solid-liquid interfaces with subnanometer-scale resolution. For the detection of water, its possibility has been well demonstrated by several research groups [14, 15, 56]. In the meanwhile, the detection of ions was not demonstrated. In this study, we demonstrated that 3D-SFM can detect ions at solid-liquid interfaces even for the ions that cannot be detected by the 2D imaging. This result marks an important step towards the establishment of the method and highlights the effectiveness of 3D-SFM for investigating the behavior of ions at solid-liquid interfaces.

Acknowledgments

This work was supported by ACT-C, Japan Science and Technology Agency; JSPS KAKENHI Grant Number JP16H02111; and CHOZEN Project, Kanazawa University. MW and AS thank the Leverhulme trust for previous funding (grant F/07 134/CK). Via our membership of the UK's HEC Materials Chemistry Consortium, which is funded by EPSRC (EP/L000202), this work used the ARCHER UK National Supercomputing Service (http://www.archer.ac.uk).

References

[1] P. Raiteri and J. D. Gale. *J. Am. Chem. Soc.*, 132(49):17623–17634, 2010.

[2] Jared Ostmeyer, Sudha Chakrapani, Albert C. Pan, Eduardo Perozo, and Benoît Roux. *Nature*, 501:121–124, 2013.

[3] Dmitriy Krepkiy, Mihaela Mihailescu, J. Alfredo Freites, Eric V. Schow, David L. Worcester, Klaus

Gawrisch, Douglas J. Tobias, Stephen H. White, and Kenton J. Swartz. *Nature*, 462:473–479, 2009.

[4] Margaret S. Cheung, Angel E. García, and José N. Onuchic. *Proc. Natl. Acad. Sci.*, 99:685–690, 2002.

[5] Guangbin Dong, Peili Teo, Zachary K. Wickens, and Robert H. Grubbs. *Science*, 333:1609–1612, 2011.

[6] S. Bae, R. Taylor, D. Hernández-Cruz, S. Yoon, D. Kilcoyne, and P. J. M. Monteiro. *J. Am. Chem. Soc.*, 98:2914–2920, 2015.

[7] A. Vorobiev, A. Dennison, D. Chernyshov, V. Skrypnychuk, D. Barbero, and A. V. Talyzin. *Nanoscale*, 6:12151–12156, 2014.

[8] G. L. Richmond. *Chem. Rev.*, 102:2693–2724, 2002.

[9] G. Binnig, C. F. Quate, and Ch. Gerber. *Phys. Rev. Lett.*, 56:930–933, 1986.

[10] T. Fukuma, K. Kobayashi, K. Matsushige, and H. Yamada. *Appl. Phys. Lett.*, 87:034101, 2005.

[11] T. Fukuma, M. J. Higgins, and S. P. Jarvis. *Phys. Rev. Lett.*, 98:106101, 2007.

[12] F. J. Giessibl. *Science*, 267:68–71, 1995.

[13] S. Kitamura and M. Iwatsuki. *Jpn. J. Appl. Phys. Part II*, 34:L145–L148, 1995.

[14] T. Fukuma, Y. Ueda, S. Yoshioka, and H. Asakawa. *Phys. Rev. Lett.*, 104:016101, 2010.

[15] K. Kobayashi, N. Oyabu, K. Kimura, S. Ido, K. Suzuki, T. Imai, K. Tagami, M. Tsukada, and H. Yamada. *J. Chem. Phys.*, 138:184704, 2013.

[16] F. Ito, K. Kobayashi, P. Spijker, L. Zivanovic, K. Umeda, T. Nurmi, N. Holmberg, K. Laasonen, A. S. Foster, and H. Yamada. *J. Phys. Chem. C*, 120:19714–19722, 2016.

[17] H. Söngen, C. Marutschke, P. Spijker, E. Holmgren, I. Hermes, R. Bechstein, S. Klassen, J. Tracey, A. S. Foster, and A. Kühnle. *Langmuir*, 33:125–129, 2017.

[18] S. M. R. Akrami, H. Nakayachi, T. Watanabe-Nakayama, H. Asakawa, and T. Fukuma. *Nanotechnology*, 25:455701, 2014.

[19] T. Fukuma, B. Reischl, N. Kobayashi, P. Spijker, F. F. Canova, K. Miyazawa, and A. S. Foster. *Phys. Rev. B*, 92:155412, 2015.

[20] M. Ricci, W. Trewby, C. Cafolla, and K. Voïtchovsky. *Scientific Reports*, 7:43234, 2017.

[21] T. Fukuma, K. Onishi, N. Kobayashi, A. Matsuki, and H. Asakawa. *Nanotechnology*, 23:135706, 2012.

[22] B. Reischl, M. Watkins, and A. S.Foster. *J. Chem. Theory Comput.*, 9:600–608, 2013.

[23] K. Miyazawa, N. Kobayashi, M. Watkins, A. L. Shluger, K. Amano, and T. Fukuma. *Nanoscale*, 8:7334–7342, 2016.

[24] M. Watkins and B. Reischl. *J. Chem. Phys.*, 138:154703, 2013.

[25] K.-I. Amano, K. Suzuki, T. Fukuma, O. Takahashi, and H. Onishi. *J. Chem. Phys.*, 139:224710, 2013.

[26] M. Ricci, P. Spijker, Francesco Stellacci, J.-F. Molinari, and K. Voïtchovsky. *Langmuir*, 29:2207–2216, 2013.

[27] M. Ricci, P. Spijker, and K. Voïtchovsky. *Nature Communications*, 5:4400, 2014.

[28] S.-H. Loh and S. P. Jarvis. *Langmuir*, 26:9176–9178, 2010.

[29] I. Siretanu, D. Ebeling, M. P. Andersson, S. L. S. Stipp, A. Philipse, M. C. Stuart, D. Ende, and F. Mugele. *Scientific Reports*, 4:4956, 2014.

[30] D. M.-Jimenez, E. Chacon, P. Tarazona, and R. Garcia. *Nature Communications*, 7:12164, 2016.

[31] A. S. Foster, C. Barth, A. L. Shluger, and M. Reichling. *Phys. Rev. Lett.*, 86:2373–2376, 2001.

[32] A. S. Foster, A. L. Shluger, and R. M. Nieminen. *Appl. Surf. Sci.*, 188:306–318, 2002.

[33] A. S. Foster, C. Barth, A. L. Shluger, R. M. Nieminen, and M. Reichling. *Phys. Rev. B*, 66:235417, 2002.

[34] A. S. Foster, A. L. Shluger, and R. M. Nieminen. *Nanotechnology*, 15:S60, 2004.

[35] N. Senguttuvan, M. Aoshima, K. Sumiya, and H. Ishibashi. *J. Cryst. Growth*, 280:462–466, 2005.

[36] I. Nicoara, M. Stef, and A. Pruna. *J. Cryst. Growth*, 310:1470–1475, 2008.

[37] Y. Zhang, X. Xiang, and W. J. Weber. *Nucl. Instr. and Meth.*, 266:2750–2753, 2008.

[38] S. Wakahara, Y. Furuya, T. Yanagida, Y. Yokota, J. Pejchal, M. Sugiyama, N. Kawaguchi, D. Totsuka, and A. Yoshikawa. *Opt. Mater.*, 34:729–732, 2012.
[39] T. Aoba and O. Fejerskov. *Crit. Rev. Oral Biol. Med.*, 13:155–170, 2002.
[40] O. Prymak, V. Sokolova, T. Peitsch, and M. Epple. *Cryst. Growth Des.*, 6:498–506, 2006.
[41] S. M. Hamza and S. K. Hamdona. *J. Phys. Chem.*, 95:3149–3152, 1991.
[42] Z. Amjad. *Langmuir*, 9:597–600, 1993.
[43] C. H. de Vreugd, J. H. ter Horst, P. F. M. Durville, G. J. Witkamp, and G. M. van Rosmalen. *Coll. Surf. A*, 154:259–271, 1999.
[44] C. Y. Tai. *J. Cryst. Growth*, 206:109–118, 1999.
[45] C. Y. Tai, . Chen P. C, and T. M. Tsao. *J. Cryst. Growth*, 290:576–584, 2006.
[46] J. J. Eksteen, M. Pelser, M. S. Onyango, L. Lorenzen, C. Aldrich, and G. A. Georgalli. *Hydrometallurgy*, 91:104–112, 2008.
[47] M. Watkins and A. L. Shluger. *Phys. Rev. Lett.*, 105:196101, 2010.
[48] Matthew Watkins, Max L Berkowitz, and Alexander L Shluger. *Physical Chemistry Chemical Physics*, 13(27):12584–12594, 2011.
[49] N. Kobayashi, S. Itakura, H. Asakawa, and T. Fukuma. *J. Phys. Chem. C*, 117:24388–24396, 2013.
[50] T. Fukuma, M. Kimura, K. Kobayashi, K. Matsushige, and H. Yamada. *Rev. Sci. Instrum.*, 76:053704, 2005.
[51] T. Fukuma and S. P. Jarvis. *Rev. Sci. Instrum.*, 77:043701, 2006.
[52] T. Fukuma. *Rev. Sci. Instrum.*, 80:023707, 2009.
[53] J. E. Sader and S. P. Jarvis. *Appl. Phys. Lett.*, 84:1801–1803, 2004.
[54] D. Bosbach, G. Jordan, and W. Rammensee. *Eur. J. Mineral.*, 7:267–276, 1995.
[55] G. Jordan and W. Rammensee. *Surf. Sci.*, 371:371–380, 1997.
[56] E. T. Herruzo, H. Asakawa, T. Fukuma, and R. Garcia. *Nanoscale*, 5:2678, 2013.